A photoelectron spectrometer for *k*-space mapping above the Fermi level

T. Greber[a)]
Physik Institut der Universität Zürich, Winterthurerstr. 190, CH-8057 Zürich, Switzerland

O. Raetzo
Institut de Physique, Université de Fribourg, CH-1700 Fribourg, Switzerland

T. J. Kreutz, P. Schwaller, W. Deichmann, E. Wetli, and J. Osterwalder
Physik Institut der Universität Zürich, Winterthurerstr. 190, CH-8057 Zürich, Switzerland

(Received 12 August 1997; accepted for publication 24 September 1997)

The setup of an electron spectrometer for angle-resolved photoemission is described. A sample goniometer offers the opportunity for angle scanned photoemission over 2π solid angle above the surface. A monochromatized high flux He discharge photon source is exploited to measure thermally populated electronic states above the Fermi level E_F. At energies greater than $E_F + 5k_BT$ the signal from a constant density of states declines below the photoelectron background caused by photons with higher energies than He Iα (21.2 eV). For He IIα (40.8 eV) the residual photoelectron background is lower and photoemission up to $6k_BT$ above E_F can be performed. Data showing two cuts through the Fermi surface of silver are presented. Furthermore the dispersion of the Shockley surface state on Ag (111) above the Fermi energy is quantified. © *1997 American Institute of Physics.* [S0034-6748(97)04512-7]

I. INTRODUCTION

Photoelectron spectroscopy provides direct insight into the electronic properties of matter.[1] If the momentum of the photon is neglected, energy and momentum conservation provide robust selection rules and permit a straightforward interpretation of the spectra. The data sets comprise emission probabilities as a function of the electron energy, emission direction, and eventually spin polarization.

The momenta of the photoelectrons can be measured in scanning the photon energy and/or in scanning the angle of detection. If no photon source with tunable energy is at hand one has to perform angle-scanned experiments. Here the parallel momentum $(\hbar k_x, \hbar k_y)$ and the final state energy E_{final} are measured. For angle-scanned photoemission experiments (ARPE) basically three spectrometer designs are available: (i) the Eastman-type display analyzer experiment where the angular photoelectron-intensity distribution is measured for a given energy simultaneously into a solid angle of about 90°,[2] (ii) the Leckey-type toroidal analyzer experiment where the angular distribution is measured for one polar cut across the hemisphere above the sample surface,[3] and (iii) the Fadley-type experiment where the sample is scanned across the hemisphere in front of an angle-resolving electron energy analyzer.[4] It is clear that parallel angular detection can reduce measuring time, the number of electrons that can be collected per unit time, however, is limited by the electron counters. If we want, e.g., to have a statistical accuracy better than 1% with an angular resolution of 1° over the full hemisphere a counter at 1 MHz has to acquire data for more than 4 min. This time is in the same order of magnitude as the time that is required for the movement of the sample across all emission directions in the hemisphere. As long as no fast variations in angular emission pattern shall be measured, the Fadley setup has to be favored since it has the best performance with respect to angular and energy resolution. It furthermore has the advantage of a fixed angle between the photon incidence and the electron detection direction.

In this article we report the setup of a Fadley-type photoelectron spectrometer that allows us to map the dispersion of thermally populated states up to $5k_BT$ *above* the Fermi level. This feature is realized by means of a monochromatized, i.e., satellite-free, high flux He discharge lamp in combination with a fully automated 2π UHV sample goniometer and a commercial electron energy analyzer with an ultimate resolution of 20 meV. The extension of electron spectroscopy to energies above the Fermi level is significant in comparison with other probes available for empty electronic states: In contrast to two-photon photoemission the dispersion up to the Brillouin zone boundary can be mapped, and compared to inverse photoemission the energy resolution is much better.

II. EXPERIMENT

The experiment is housed in a commercial VG Escalab 220 spectrometer where a base pressure below 10^{-8} Pa is achieved by means of a 200 l/s turbomolecular pump, an ion getter pump, and rare earth evaporators. These rare earth evaporators have superior performance compared to that of commercial Ti getter pumps since the films remain active for several weeks. The samples can be prepared by sputtering and heating to 1300 K, and characterization is possible by thermal desorption spectroscopy, low energy electron diffraction, x-ray photoelectron spectroscopy, and x-ray photoelectron diffraction.[5] In this article, we report data from Ag (111) that was cleaned by sputtering and annealing cycles to 600 K.

[a)]Electronic mail: greber@physik-rzu.unizh.ch

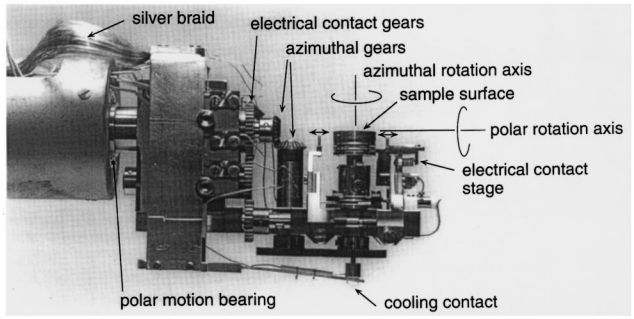

FIG. 1. Sideview of the 2π sample goniometer head. The polar rotation axis is in the horizontal direction and lies in the sample surface where it crosses the azimuthal rotation axis (vertical direction). At the bottom of the azimuthal axis the cooling contact that is electrically isolated by a sapphire sphere can be seen.

III. ANALYZER

The 180° hemispherical analyzer is equipped with a 6 channeltron detector and a versatile input lens system. We currently achieve an ultimate energy resolution of 20 meV full width at half-maximum (FWHM) as measured from He I excited Ar $3p$ gas phase spectra. The energy resolution and the transmission are proportional to the analyzer pass energy down to 35 meV (FWHM) from where the transmission starts to die off nonlinearly. The angular resolution can be varied by means of two iris apertures from 12° solid angle to below 1° FWHM.

IV. MANIPULATOR

The 2π sample goniometer is based on the Fadley design.[4] All emission angles from the sample surface can be reached. In spherical coordinates the polar emission angle θ is the angle between the electron detection direction and the surface normal, and the azimuthal emission angle ϕ is the angle between the projection of the detection direction on the surface and an arbitrary chosen direction in the sample surface.

The goniometer is designed for *in situ* sample exchange.[5] The mobile sample holders with a height of 18 mm and a diameter of 16 mm contain individual resistive heaters.

The photograph in Fig. 1 shows a side view of the manipulator head as used in our setup. The required mechanical and vacuum performance is attained by the use of bronze (CuSn12) high-precision gears and stainless steal ball bearings. The mechanical precision allows us to place samples reproducibly within less than 1°. In relative measurements the precision of the angular settings is 0.1°, limited by the steps of the stepper motors and the external gear boxes that control the two angular settings via rotary drives. For the sake of precision all angle scans are performed in one particular sense of rotation. This implies that all electrical and thermal contacts have to be sliding. The cooling system consists in a two-stage setup where the outer cycle cools the thermal shield (not shown in Fig. 1) and provides a homogeneous manipulator temperature of about 200 K. The cooling contact of the inner cycle is mounted in the azimuthal rotation axis of the sample and consists in a conical copper bolt that is pressed from below against the sample head by a sapphire isolated tungsten spring. Cooling with liquid nitrogen leads to a sample temperature of 120 K. With liquid He we reach sample temperatures below 60 K. The heat exchange between the cooling liquid and the heat conductor is optimized by porous sintered metal. On the manipulator the samples can be heated up to 800 K. The temperature is measured inside the copper bolt by a tubed thermocouple of 0.5 mm diameter. The sample temperature is calibrated by comparing with the reading of a thermocouple that is spot welded on the sample.

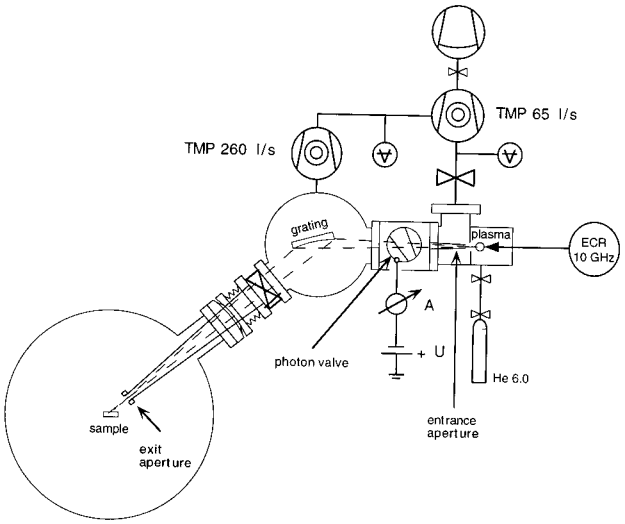

FIG. 2. Experimental setup of the UV lamp and the monochromator.

V. UV SOURCE

As UV light source a Baltzer type VUV 5000 He discharge lamp with monochromator (Gammadata Burklint AB, Sweden) is used.[6] The He discharge lines are selected and refocused on the sample by a toroidal grating monochromator. The reflectivity of the grating from Jobin Yvon is optimized for 40 eV radiation. The monochromator was originally designed for gas phase experiments and was adopted for the angle scanned photoemission experiment from surfaces in our laboratory. The electron cyclotron resonance (ECR) plasma light source and the monochromator were tuned to a maximum photon flux with a minimum of gas load in the analysis chamber. In Fig. 2 the schematic setup of the UV source is shown. In order to minimize plasma induced cracking of hydrocarbons on the Pt coated grating the source is equipped with an oil-free vacuum system. Two differential pumping stages provide a final He partial pressure in the analysis chamber of 2×10^{-6} Pa. The first pumping stage is run by a 50 l/s drag turbomolecular pump where the lamp operates optimally at an He gas pressure of 8×10^{-2} Pa. The second stage is run by a 200 l/s turbomolecular pump with the backing line connected to the ventilation port of the first turbomolecular pump. In order to minimize the He flux at a given photon flux the aperture between the first and the second pumping stage is worked as a conical nozzle where the inlet with a diameter of 2 mm is placed 3 mm away from the exit slit of the plasma source.

TABLE I. Performance of the UV source. The value of 1.0 corresponds to 1.7×10^{13} photons/s or 2×10^{12} photons/s mm^2 on the sample.

Energy (eV)	He Iα 21.2	He Iβ 23.1	He Iγ 23.7	C III 21.6	He IIα 40.8
Zero order	0.89	0.06	0.01		0.05
First order He I	0.28	0.000 25	0.000 06	0.0014	0.000 31
First order He II	<0.007				0.14

The solid angle of 8° provides complete illumination of the grating. The exit aperture on which the monochromatized light is focused has a diameter of 3 mm and corresponds to the magnification of the toroidal grating. In order to gain another factor of 2 in the final residual He pressure this aperture is worked as a cylinder with a length of 3 mm. Since the exit aperture is electrically isolated, the resulting photo-induced charging then minimizes the flux of electrons from the lamp onto the sample.

The UV source is equipped with a photon flux monitor labeled ''photon valve'' in Fig. 2. It is a rotable aperture worked from aluminum. This allows us to continuously vary the photon flux from zero to the maximum and to protect the grating from unwanted exposure in the startup phase or during sample preparation. The photon valve is electrically isolated and can therefore be used as a collector or emitter for charged particles or as a flux monitor. In biasing the photon valve with -30 V we read a maximum current of typically 8 μA of negative particles emitted from the closed aperture. In comparing the He pressure dependence of the current from the photon valve with the photocurrent from a sample after the monochromator we find that at the optimum operating conditions of the lamp about 50% of the current from the photon-valve stem from the deexcitation of metastable He atoms. This high portion of metastables indicates that He expands freely from the plasma ball in the lamp without collisions with the wall.

The photons impinge on the sample at an angle of 58° relative to the detection direction and 50° relative to the polar rotation axis of the sample. The diffraction plane of the monochromator grating is normal to the plane that is spanned by the electron detection direction and the photon incidence. This geometry therefore maximizes the p-polarized light component in the photoemission experiment.

The stability of the lamp is very high. After a start up phase of typically 30 min the photon flux is stable within 1% for one day. Therefore data may be acquired in a single scan. The clystron dc power supply on the other hand induces under load a saw tooth like variation of the photon flux of 4% with a frequency of 100 Hz. This limits the statistical accuracy for count rates above 5×10^4 counts/s. The electron counters can, however, be easily synchronized with the phase of the ac current that feeds the clystron power supply.

The radiation characteristics for the different monochromator settings are summarized in Table I. For zero order diffraction we find a photo current of 305 nA from a piece of aluminum. From the size of the light spot and the quantum efficiency of 11.3% for the emission of photoelectrons[7] the photon flux of 2×10^{12} photons/s mm^2 is derived. The values in Table I are given relative to this number and are calculated from the intensity that correspond to the intensity at the Fermi level of silver at the particular photon energies. The monochromatized light intensity on the sample is then 5×10^{12} photons/s for He Iα (21.2 eV) and 2.4×10^{12} photons/s for He IIα (40.8 eV) on a spot with a diameter of 3 mm. In addition to the high intensity the source has a high monochromaticity. For He Iα radiation we can suppress higher energy He radiation from 11% in zero order diffraction by more than a factor of 50. The most prominent ''contamination'' line with an energy larger than He Iα is C III radiation at an energy of 21.59 eV. It is, however, expected that this contribution can be reduced in replacing the pole pieces in the plasma source by highest purity iron. It has to be noted that the high intensity of the ECR plasma source allows as well the utilization of He Iβ (23.1 eV) and He IIβ radiation (48.1 eV). They are, however, about one order of magnitude weaker than the corresponding α main lines. The high photon fluxes Φ yield ''ionization times'' $\tau=1/\Phi\sigma$ in the order of 1 h with typical photoemission cross sections σ of 10 Mb in this energy regime. This may give a limit for the observation time of surfaces that are sensitive to UV radiation.

VI. RESULTS AND DISCUSSION

In Fig. 3 Fermi energy intensity maps from Ag (111) are shown for He Iα, and He IIα excited photoelectrons. In this data recording mode the electron energy is kept fixed at the Fermi energy and the azimuthal and polar emission angles are scanned. The photoelectron intensity is displayed in a linear gray scale where white corresponds to maximum intensity. The emission angle is displayed in polar coordinates (ρ,ϕ) where ϕ corresponds to the azimuthal angle and $\rho\propto\sin(\theta)$ to the parallel component of the photoelectron current momentum. The data sets comprise 2640 individual angular settings evenly spaced over a solid angle of 120°. Both Fermi maps were recorded in less than 1 h. The analyzer resolution was 35 meV for the He I scan and 90 meV for the He II scan. The angular resolution for these spectra was about 5°. The application of monochromatized, i.e., satellite-free radiation, ensures that the observed features are intrinsic for the corresponding radiation energy.

Most features observed in Fig. 3 can be rationalized in terms of resonant transitions from occupied states at the Fermi level to unoccupied states on a free-electron-like final state sphere. This is shown in Fig. 4 where a cut in k-space that comprises Γ_{000}, Γ_{111}, and Γ_{002} is shown. The initial states are mimicked by circles that correspond to cuts across the Fermi spheres centered at the Gamma points. For simplicity the ''necks'' that connect the Fermi spheres of different Brillouin zones at the L points are omitted. The free-electron final states are indicated by circles around Γ_{000} with radii $k_{\text{final}}=1/\hbar\sqrt{\hbar\omega-\Phi+U}$, where $\hbar\omega$ is the photon energy, Φ is the work function, and U the inner potential of the sample. All intersections between the initial and the final states lead to direct transitions and correspondingly to high intensity in the k scan. This can be inspected by eye in Fig. 3 where, e.g., circular contours centered at Γ_{00} correspond to direct transitions from the Fermi sphere around Γ_{111}. All this

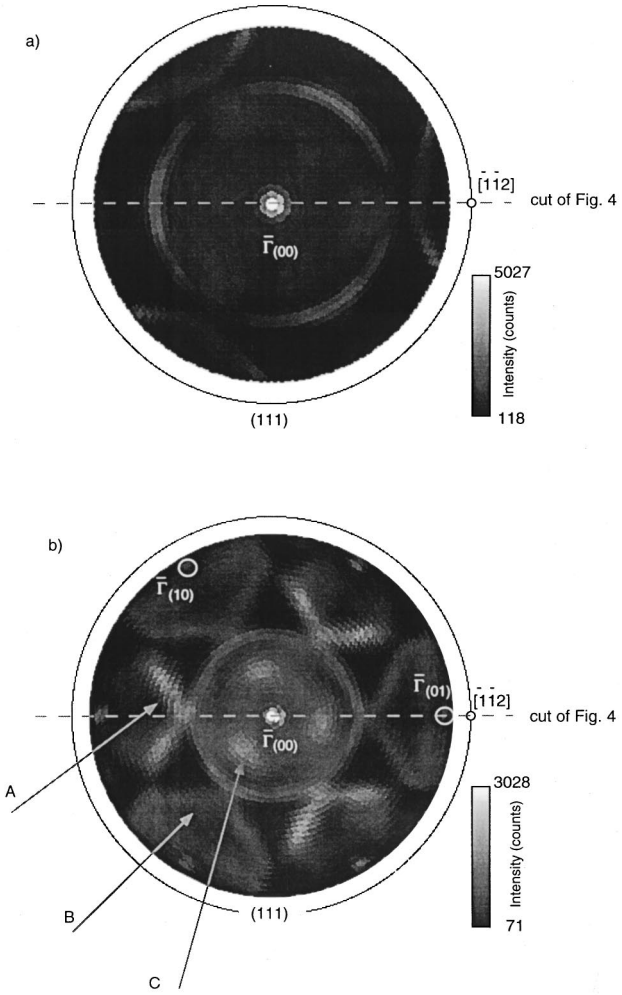

FIG. 3. Fermi surface maps from Ag (111). (a) He I (21.2 eV) at 300 K and (b) He II (40.8 eV) excited at 140 K.

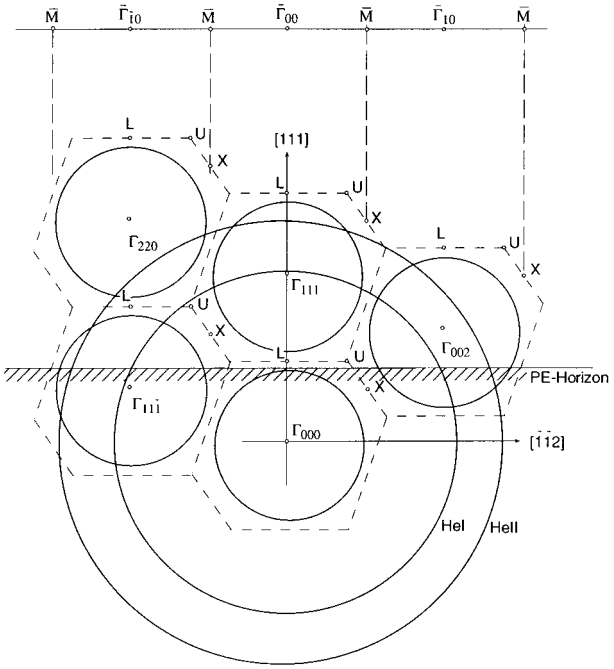

FIG. 4. Cut across the extended Brillouin zone scheme of Ag in k space. A plane containing the surface normal and the [112] direction is shown. Direct transitions are expected for all intersections of initial states with final states. For simplicity all states are assumed to be free-electron-like. They can therefore be displayed as cuts across spheres with radii $k=1/\hbar\sqrt{2mE_{\mathrm{kin}}}$. The PE horizon is the photoemission threshold given by the inner potential of the sample.

has been discussed for the case of copper where it was shown that this way of displaying the data maps the Fermi surface at a particular final state momentum $\hbar k_{\mathrm{final}}$.[8]

The Shockley surface state at normal emission, which is not part of the bulk band structure (Fig. 4), is the most prominent feature in the data of Fig. 3. In the case of the He II scan [Fig. 3(b)] the centers of the second surface Brillouin zones can be observed and they show intensity from the surface states as well. Here surface umklapp processes of bulk Fermi surface features can also be observed. This is reflected in the six V-shaped features (A and B) that touch the Γ_{111} Fermi sphere (cf. also Fig. 4). The features A are identified as the intersections of the He II final state sphere with the Fermi spheres centered at Γ_{220}, Γ_{202}, and Γ_{022} and the weaker features B as the umklapps of A. If no surface umklapp processes would be at work, they would produce a three-fold rotational symmetry around Γ_{00}.

From the data of Fig. 3(b) it becomes clear that not only direct transitions and umklapp processes contribute to the Fermi surface maps. The three broad peaks inside the Γ_{111} Fermi sphere (labeled C) cannot be explained by direct transitions. The purity of our radiation source excludes satellites to be responsible for these quite strong features. Upon closer inspection they are azimuthally rotated relative to the high-symmetry directions and break the mirror symmetry of the sample. This clues the polarization of the obliquely incident light to be reflected in these features. Within the three-step model of photoemission we therefore assign them to elastic final state scattering in the second step, i.e., the transport of

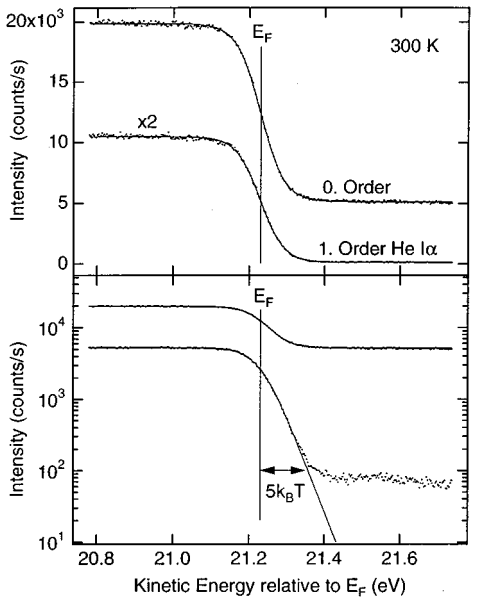

FIG. 5. Electron distribution curves with an energy resolution of 50 meV from the Fermi level of a silver sample; (a) on a linear scale and (b) on a logarithmic scale. The bottom panel shows that with the monochromatized source the Boltzmann wing can be measured up to $5\,k_BT$ above the Fermi level.

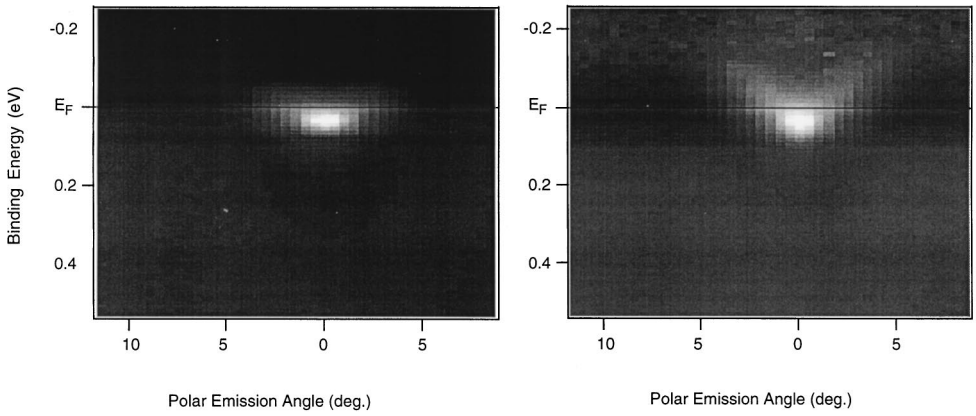

FIG. 6. $E(k)$ scan across the surface normal of Ag (111). The bright feature corresponds to the Shockley surface state. In (a) the discontinuity of the photoemission intensity at the Fermi level can be seen. In (b) this discontinuity is removed in normalizing the $k(E)$ scans with the average intensity at a given energy. After this procedure the dispersion can be observed from the raw data up to $5\,k_BT$ above the Fermi level.

the photoelectron to the surface. Similar polarization effects have been observed in energy-integrated ARPES patterns of $3d$ emission from copper surfaces.[9]

For the electronic properties of a solid the dispersion near the Fermi level is most important. Although Fermi surface maps provide important information on the electronic properties of the surface under investigation they do not furnish direct information on the dispersion of the electronic states at the Fermi level. It is, however, crucial to know the band dispersion precisely if, e.g., phase transitions shall be understood on a microscopic level. Photoemission cooperates with this interest with respect to momentum and energy resolution since lifetime broadening is minimal at the Fermi energy. Above the Fermi level the photoemission contrast is highest but the photoemission intensity dies off as does the population of the electronic states. If one wants to measure electronic states above the Fermi level, high intensity and monochromaticity are equally important for the experiment. A monochromator has to provide a minimum of photons with energies higher than that at which the Fermi level is measured since this higher energy radiation causes unwanted electron emission above the Fermi level. The photon source described in this article permits photoemission up to $5\,k_BT$ above the Fermi level. For He IIα (40.8 eV) the residual photoelectron background is lower and photoemission up to $6\,k_BT$ above E_F can be performed. In Fig. 5 the photoemission intensity from silver excited with He Iα radiation is shown in an energy window around the Fermi level. In plotting the data on a semilogarithmic scale it is shown that with the monochromatized He Iα radiation the Boltzmann wing of the Fermi Dirac distribution can be measured up to $5\,k_BT$ above the Fermi level. For comparison the spectrum with nonmonochromatized zero-order He Iα radiation is shown. With He Iα radiation the same criterion leads to an upper photoemission cutoff of $6\,k_BT$ since higher energy satellites are less prominent for this radiation.

In order to demonstrate the capability for **k**-resolved photoemission above the Fermi level, i.e., the measurement of thermally excited electrons, the energy-momentum relation of the Ag (111) Shockley surface state is plotted in Fig. 6. Photoelectron spectra taken in polar angle steps of 0.5° across the surface normal and near the Fermi level are displayed. The photoemission intensity increases from black to white in a linear gray scale. The polar emission angle is related to the parallel component of the electron momentum. On the left panel the discontinuity in intensity at the Fermi level can be observed. The bright feature around $\theta=0°$ stems from transitions from the surface state. On the right panel the data at each energy have been normalized by the average intensity of all angles at that energy. As a consequence the parabolic dispersion of the surface state that indicates free-electron-like behavior can be detected even 100 meV above the Fermi level. The binding energy E_B and the effective mass m^* of this band can thus be very accurately determined. In this kind of data set one does not rely on the knowledge of the experimentally observed Fermi function since for the determination of the dispersion the peaks in the angle scan for each individual energy can be used.[10] At the $\overline{\Gamma}$ point $E_B(300\ \mathrm{K})=21\pm2$ meV and $m^*=0.30\pm0.02\,m_e$ is found for the surface state. The result for the binding energy agrees with that determined by Matzdorf *et al.* (25 meV).[11] The effective mass, however, turns out to be smaller than the value reported in Ref. 11 $(0.45\pm0.04\,m_e)$. This disagreement may be due to the extended k-space range above the Fermi level in which we observe the surface state. It may be as well differences of the sample since the authors of Ref. 11 claim as well to have evaluated the dispersion up to $5\,k_BT$ above the Fermi level.

VII. DISCUSSION

The setup of a new instrument for advanced photoemission is reported. It is now possible to map thermally excited states $5\,k_BT$ above the Fermi level up to the Brillouin zone boundary. The measurement of high parallel momentum electronic states with high energy and momentum resolution should be particularly useful for the observation of the interplay between electrons and phonons.

[1] S. Hüfner, *Photoelectron Spectroscopy*, Springer Series in Solid-State Science (Springer, Berlin, 1995).
[2] D. E. Eastman, J. J. Donelon, N. C. Hien, and F. J. Himpsel, Nucl. Instrum. Methods **172**, 327 (1980).

[3] R. C. G. Leckey and J. D. Riley, Appl. Surf. Sci. **22/23**, 196 (1985).
[4] C. S. Fadley, Prog. Surf. Sci. **16**, 275 (1984).
[5] J. Osterwalder, T. Greber, A. Stuck, and L. Schlapbach, Phys. Rev. B **44**, 13 764 (1991).
[6] P. Baltzer, L. Karlsson, M. Lundqvist, and B. Wanneberg, Rev. Sci. Instrum. **64**, 2179 (1993).
[7] R. B. Cairns and J. A. R. Samson, J. Opt. Soc. Am. **56**, 1568 (1966).
[8] P. Aebi, J. Osterwalder, R. Fasel, D. Naumovic, and L. Schlapbach, Surf. Sci. **307–309**, 917 (1993).
[9] J. Osterwalder, T. Greber, P. Aebi, R. Fasel, and L. Schlapbach, Phys. Rev. B **53**, 10 209 (1996).
[10] T. J. Kreutz, P. Aebi, and J. Osterwalder, Solid State Commun. **96**, 339 (1995).
[11] R. Paniago, R. Matzdorf, G. Meister, and A. Goldmann, Surf. Sci. **336**, 113 (1995).